Available online at www.sciencedirect.com
SCIENCE DIRECT
Journal of Power Sources 157 (2006) 816–827
JOURNAL OF POWER SOURCES
www.elsevier.com/locate/jpowsour

Dynamic modelling and hardware-in-the-loop testing of PEMFC

Andreas Vath [a,*], Zijad Lemeš [b], Hubert Mäncher [b], Matthias Söhn [a], Norbert Nicoloso [a], Thomas Hartkopf [a]

[a] *Technische Universität Darmstadt/Institut für Elektrische Energie wand lung, Landgraf-Georg-Str. 4, D-64283 Darmstadt, Germany*
[b] *MAGNUM Automatisierungstechnik GmbH, Bunsenstr. 22, D-64293 Darmstadt, Germany*

Received 14 October 2005; received in revised form 23 February 2006; accepted 23 February 2006

Abstract

Modelling and hardware-in-the-loop (HIL) testing of fuel cell components and entire systems open new ways for the design and advance development of FCs. In this work proton exchange membrane fuel cells (PEMFC) are dynamically modelled within MATLAB-Simulink at various operation conditions in order to establish a comprehensive description of their dynamic behaviour as well as to explore the modelling facility as a diagnostic tool. Set-up of a hardware-in-the-loop (HIL) system enables real time interaction between the selected hardware and the model.

The transport of hydrogen, nitrogen, oxygen, water vapour and liquid water in the gas diffusion and catalyst layers of the stack are incorporated into the model according to their physical and electrochemical characteristics. Other processes investigated include, e.g., the membrane resistance as a function of the water content during fast load changes. Cells are modelled three-dimensionally and dynamically. In case of system simulations a one-dimensional model is preferred to reduce computation time. The model has been verified by experiments with a water-cooled stack.

Keywords: PEM fuel cell; Dynamic modelling; Hardware-in-the-loop; Test benches; Fuel cell vehicle

1. Introduction

By means of mathematical modelling the development and design of fuel cell systems can be significantly accelerated. To optimise and develop the fuel cell hardware first a detailed description of a PEMFC three-dimensional model is given. In case of system simulations and HIL applications with regard to computational time a one-dimensional PEMFC model is used. Both the three-dimensional as well as one-dimensional model are implemented in MATLAB/Simulink.

The main model outputs are cell voltage, temperature as well as electrical and thermal power, which are calculated with respect to different operating conditions, such as load current, pressure, flow, gas composition, moisture, etc. The model uses basic electrochemical and physical principles with special emphasis on the description of dynamic behaviour.

The vehicle model consists of the commercially available simulation tool CarSim where the internal combustion engine is replaced by a model of an asynchronous motor and an inverter.

After the model-based analysis the hardware-in-the-loop (HIL) vehicle system is introduced, which allows to investigate the behaviour of the real components in a virtual environment. The main components of the fuel cell HIL system, their properties will be described in detail below, are the command station, target node PC with real time operating system, signal-conditioning unit, device under test and, for presentation purposes, a separate human machine interface consisting of a steering-wheel and a break and throttle pedal.

2. Three-dimensional fuel cell model

The dynamic PEFC three-dimensional model (Fig. 1) includes the flowfield, gas diffusion layer (GDL), catalyst layer of the anode and cathode as well as the membrane. The model has been implemented in MATLAB/Simulink software and the simulation can run with discrete or continuous time steps.

The number of elements in each direction can be chosen freely with exception of the catalyst, which is modelled as a border layer and the flowfield. The flowfield is modelled only in x–y direction, because the gases have to follow the gas channels and so the gas composition is changing mainly along

* Corresponding author. Tel.: +49 6151 163167; fax: +49 6151 166074.
E-mail address: andreas.vath@re.tu-darmstadt.de (A. Vath).

0378-7753/$ – see front matter © 2006 Elsevier B.V. All rights reserved.
doi:10.1016/j.jpowsour.2006.02.102

Nomenclature

α_{An}	Anode charge transfer coefficient (–)
α_{Ca}	Cathode charge transfer coefficient (–)
ε_{GDL}	Porosity GDL (–)
μ	Potential (V)
λ	Membrane water content (–)
A	Cell area (m^2)
c_i	Molar concentration of component i ($mol\,m^{-3}$)
d	Width of the membrane (m)
D_i	Diffusive coefficient of component i (–)
E	Activity coefficient (–)
F	Faraday constant ($C\,mol^{-1}$)
ΔG^0	Gibbs energy ($J\,mol^{-1}$)
i	Current density ($A\,cm^{-2}$)
$j_{0,An}$	Exchange current density anode ($A\,cm^{-2}$)
$j_{0,Ca}$	Exchange current density cathode ($A\,cm^{-2}$)
J_i	Diffusive flux of component i ($mol\,m^{-2}\,s^{-1}$)
k	Proton conductivity ($S\,m^{-1}$)
M_i	Molar mass (kg)
n_i	Mass (mol)
$\dot{n}_i$	Mass flow rate ($mol\,s^{-1}$)
N_i	Molar flux of component i ($mol\,m^{-2}\,s^{-1}$)
p_i	Partial pressure of component i (pa)
R	Gas constant ($j\,mol^{-1}\,K^{-1}$)
R_{El}	Electric resistance ($\Omega\,cm^2$)
R_{mem}	Ionic resistance ($\Omega\,cm^2$)
s	Swelling factor (–)
t	Time (s)
t_w	Transport number (–)
T	Cell temperature (K)
T^0	Reference temperature (K)
U_O	Open cell voltage (V)
U_{An}	Anode voltage losses (V)
U_{Ca}	Cathode voltage losses (V)
U_{cell}	Cell voltage (V)
U_Ω	Ohmic voltage loss (V)
u^m	Mixture velocity ($m\,s^{-1}$)
V	Volume (m^3)
x	Mol fraction (–)
z	Length (m)

this direction. The flow-field could be a linear one or a meander type and it is possible to chose the direction of the anode and cathode flow in linear, counter or cross. The pressure and the gas composition is changing along the channel depending on the current density in each simulated element.

The gas diffusion layer incorporates the gas transport from the flowfield to the catalyst layer and the removal of the reactants. Here the transport of liquid water is also included. For the catalyst layer the main electrochemical processes are considered. The mentioned fuel cell components and especially the membrane and their influence on the performance could be analysed in detail.

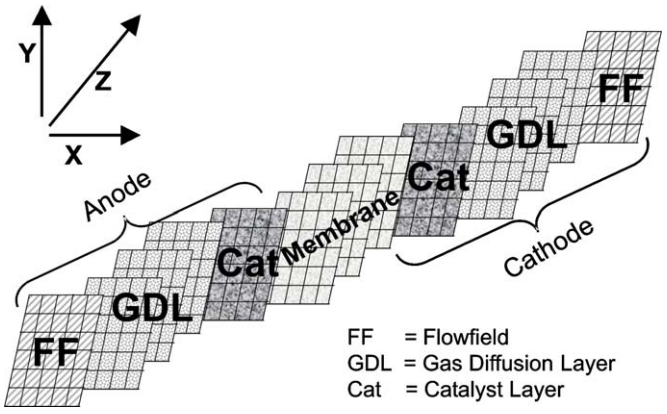

Fig. 1. Fuel cell model.

2.1. Flowfield

After inlet the gases have to follow the channels through the flowfield plate. For computational convenience the gases are supposed to obey the ideal gas law. At the anode H_2, H_2O and at the cathode O_2, N_2, H_2O are considered. The pressure distribution of all gas components and the whole pressure is calculated along the gas channels. This is influenced by the transported species via concentration and pressure gradients of the processes in the GDL, which are explained in detail in the next paragraph.

2.2. Gas diffusion layer

Gas diffusion layers serve as current collectors allowing ready access of the fuel and oxidant to anode and cathode catalyst surfaces, respectively. A gas diffusion layer usually contains a mixture of carbon black powder, hydrophobic dispersion agent, and solvents, applied onto carbon paper or woven carbon cloth substrates (both have macropores), to form a uniform thin microporous layer on top of the macroporous layer of the substrates. Here, gas diffusion layers are manufactured using Toray papers as the macroporous substrate.

In the model, the main input parameters of the GDL anode and the GDL cathode are:

- i, current density,
- T, temperature,
- P_{H_2}, P_{O_2}, P_{N_2}, P_{H_2O}, partial pressures, and
- geometric and material characteristics.

In the following, the calculations of the GDL on the basis of reference [1] will be explained. The diffusive transport is modelled using Fick's first law. However, it is strictly valid only for binary mixtures and for some mixtures of three or more components, the Maxwell–Stefan equations are required to obtain reliable results.

The governing equations for the gas mixture will be described by the concentration c_i in the subsequent equations. The next table presents the values that c_i takes in the anode and in the cathode. The conservation of mass for the gas mixture takes the form of the Eq. (1). The evaluation is made using the ODE

Matlab functions.

$$\frac{\partial c_i}{\partial t} = -\nabla N_i = -\nabla(J_i + c_i u^{\mathrm{m}}) \tag{1}$$

where u^{m} is the molar-averaged mixture velocity and J_i the diffusive flux (measured relative to the molar-averaged velocity). Eq. (1) describes the total convective plus diffusive flux of each gas. The diffusive flux is given by Fick's law, which states that the flux of one component relative to the molar-averaged velocity is proportional to the gradient in mole fractions via,

$$J_i = \Delta c_i D_i A \frac{\varepsilon_{\mathrm{GDL}}}{\Delta \mathrm{z}} \tag{2}$$

where the diffusion coefficient D_i is given by,

$$D_i = \left(1 - \frac{p_i}{p_{\mathrm{MIX}}}\right) \frac{1}{\sum\limits_{\substack{k \\ k \neq i}} (p_k / p_{\mathrm{MIX}})} \tag{3}$$

The second term of Eq. (1) is the convective term:

$$c_i u^{\mathrm{m}} = \Delta c_i \Delta p_{\mathrm{MIX}} A \frac{\varepsilon_{\mathrm{GDL}}}{\Delta z} \tag{4}$$

In both Eqs. (2) and (4) the porosity $\varepsilon_{\mathrm{GDL}}$ is represented by:

$$\varepsilon_{\mathrm{GDL}} = \frac{M_{\mathrm{H_2O}} n_{\mathrm{H_2O^{liq}}}}{\rho_{\mathrm{H_2O^{liq}}} \Delta V} \tag{5}$$

$M_{\mathrm{H_2O}}$ and $\rho_{\mathrm{H_2O^{liq}}}$ are the molar mass and the density of the water respectively, and finally is the ΔV volume of the GDL. The pressure of the mixture p_{MIX} is evaluated assuming the gas to be ideal and adiabatic. It depends linearly on the concentration.

$$p_{\mathrm{MIX}} = \sum_i p_i \tag{6}$$

where p_i is the partial pressure of each gas,

$$p_i = c_i RT \tag{7}$$

R is the universal gas constant and T the temperature. Although there are significant temperature variations within a fuel cell, the model considers the system to be isothermal.

2.3. Catalyst layer

For the catalyst layer the main gas transport equations as in the GDL are included. A sink term is used to account for depletion of oxygen at the cathode and depletion of hydrogen at the anode. The electrochemical and physical processes are complex at the catalyst layer. First-order kinetics is assumed using the Bulter–Volmer equation. For the liquid water mass conservation equation, the source terms at the cathode and anode are respectively:

$$\dot{n}_{\mathrm{H_2}} = \frac{i}{2F} A \tag{8}$$

$$\dot{n}_{\mathrm{O_2}} = \frac{i}{4F} A \tag{9}$$

$$\dot{n}_{\mathrm{H_2O}} = \frac{i}{2F} A \tag{10}$$

where i is the current density and A the area of the membrane.

2.4. Membrane

The amount of water fed into the cell by humidified reactant gases depends on the gas temperature, pressure and flow rate, whereas water production on the cathode depends mainly on the current density, to which it is directly proportional. In a PEM fuel cell water is transported along the gas channels, but also through the membrane and the electrodes. Transport processes, which are schematically represented in Fig. 2, occur in an ionomere membrane.

For the water transport, the principles driving modelled forces are:

- Convective force
- Osmotic force or diffusion
- Electric force

The first of these forces arises from a pressure gradient, the second from a concentration gradient, and the third from the migration of protons from anode to cathode and their effect (drag) on the dipole water molecules. For water and protons the mass conservation equation can be represented as:

$$\frac{\mathrm{d}c_i}{\mathrm{d}t} = -\nabla N_i, \quad i = \mathrm{H_2O},\ \mathrm{H^+} \tag{11}$$

where c_i is the molar concentration and N_i the molar flux due to electro-osmotic driving forces and convection. The molar flux can be represented as:

$$N_i = J_i + c_i u^m \tag{12}$$

where u^{m} is the mixture velocity and J_i the diffusive flux. In the model, the diffusive flux for the water and the proton current is calculated on the bases of [2] as:

$$J_{\mathrm{H_2O}} = \left(-\frac{t_w k}{F^2} \frac{\partial \mu_{\mathrm{H^+}}}{\partial z} - \frac{D_w c_{\mathrm{H_2O}}}{RT} \frac{\partial \mu_{\mathrm{H_2O}}}{\partial z}\right) \frac{1}{1 + s\lambda} \tag{13}$$

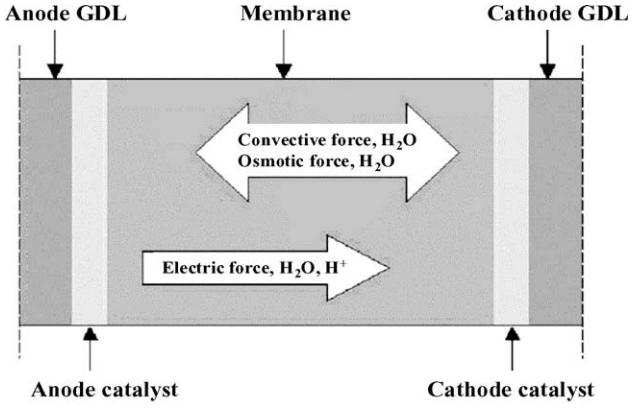

Fig. 2. Direction of the water transport forces inside the membrane.

$$J_{H^+} = \left(-\frac{k}{F^2}\frac{\partial \mu_{H^+}}{\partial z} - \frac{t_w k}{F^2}\frac{\partial \mu_{H_2O}}{\partial z} \right) \frac{1}{1+s\lambda} \tag{14}$$

The potential gradient from water is calculated through:

$$\frac{\partial \mu_{H_2O}}{\partial z} = \frac{RT}{x_{H_2O}}\frac{\partial x_{H_2O}}{\partial z} \tag{15}$$

Inserting the Eqs. (14) and (15) in (13)

$$J_{H_2O} = \left(-J_{H^+} t_w (1+s\lambda) + \frac{t_w^2 k}{F^2}\frac{RT}{x_{H_2O}}\frac{\partial x_{H_2O}}{\partial z} - \frac{D_w c_{H_2O}}{x_{H_2O}}\frac{\partial x_{H_2O}}{\partial z} \right) \frac{1}{1+s\lambda} \tag{16}$$

where the transport number for Nafion® is evaluated as:

$$t_w = 2.5\frac{\lambda}{22} \tag{17}$$

where in

$$\lambda = \frac{n_{H_2O}}{n_{SO_3H}} \tag{18}$$

with $n_{SO_3H} = 1.8634 \times 10^3\ \mathrm{mol/m^2}$

The swelling factor takes the value $s = 0.0123$.

The temperature dependence of k is calculated with:

$$k = k_{ref} e^{-E_{A,K}((1/T)-(1/T_{ref}))} \tag{19}$$

where $T_{ref} = 353.15\ \mathrm{K}$ and K_{ref} is given by:

$$k_{ref} = 0.0013\lambda^3 + 0.0298\lambda^2 + 0.2568\lambda \tag{20}$$

In (19) the coefficient of activity appears, which is calculated as:

$$E_{A,K} = 2640 e^{-0.6\lambda} + 1183 \tag{21}$$

The diffusion coefficient is calculated by the expression:

$$D_w = 21\lambda e^{(-2436/T)} \tag{22}$$

The molar fractions are:

$$x_{H_2O} = \frac{\lambda}{\lambda+2} \qquad x_{H^+} = \frac{1}{\lambda+2} \tag{23}$$

The concentration of the water is:

$$c_{H_2O} = \frac{n_{H_2O}}{V} \tag{24}$$

where V is the volume of the membrane. The current is given by the flow of protons:

$$J_{H^+} = \frac{i}{F} \tag{25}$$

The resistance of the membrane corresponds to:

$$R_{Mem} = \frac{d}{k} \tag{26}$$

where d is the width of the membrane and k is calculated by Eq. (19).

2.5. Cell voltage

The cell voltage is described by the following equation:

$$U_{cell} = U_O - U_{An} - U_\Omega - U_{Ca} \tag{27}$$

where U_O is the open cell voltage, U_{An} and U_{Ca} are the voltage losses on anode and cathode side, respectively, and U_Ω represents the ohmic losses due to ionic conductivity of the membrane and due to electronic conductivity of bipolar plates, diffusion and catalyst layers.

The open cell voltage is a function of temperature and partial pressures of reactants and is calculated as follows:

$$U_O = -\frac{\Delta G^0}{2F} + \frac{\Delta S}{2F}(T - T^0) + \frac{RT}{2F}\left(\frac{1}{2}\ln\frac{p_{O_2}}{p^0} + \ln\frac{p_{H_2}}{p^0} \right) \tag{28}$$

Based on the Bulter–Volmer equation [3], which describes the reduction and oxidation processes on the electrode, and neglecting the opposite reaction on each electrode, the losses through the charge transfer can be described as follows:

$$U_A = \frac{RT}{(\alpha_{An} + \alpha_{Ca})F}\frac{i}{i_{0,An}} \tag{29}$$

$$U_{Ca} = \frac{RT}{\alpha_{Ca} F}\ln\frac{i}{i_{0,Ca}} \tag{30}$$

The exchange current density i_0 and transfer coefficient α are measures for the reaction kinetics. The exchange current density is concentration and temperature dependent. Since the exchange current density for the hydrogen electrode is considerably higher than oxygen, charge transfer losses at the anode are small and may be neglected.

Ohmic losses, mainly associated with the membrane part, are given by the following equation:

$$U_\Omega = R_{El} i + R_{Mem} i \tag{31}$$

where R_{El} represents the losses through the electronic conductivity and R_{Mem} the voltage loss due to ionic conductivity of the membrane. The conductivity of the membrane depends on temperature and water content [4].

Because of the low charge transfer resistance the resulting time constant is also small. Therefore, the double layer capacitance on the anode side can be neglected.

2.6. Simulation results

The dynamic results of the 3D fuel cell model are shown in this chapter and compared with the experimental results. The measurement was done with a water-cooled stack within five cells. The active area was 100 $\mathrm{cm^2}$ and the membrane type used was GORE PRIMEA MESGA with a thickness of 35 μm. The GDL employed was SIGRACET GDL, GDL-10 BB, 420 μm. The meander type flowfield with a depth of 1.3 mm was used in parallel counter flow.

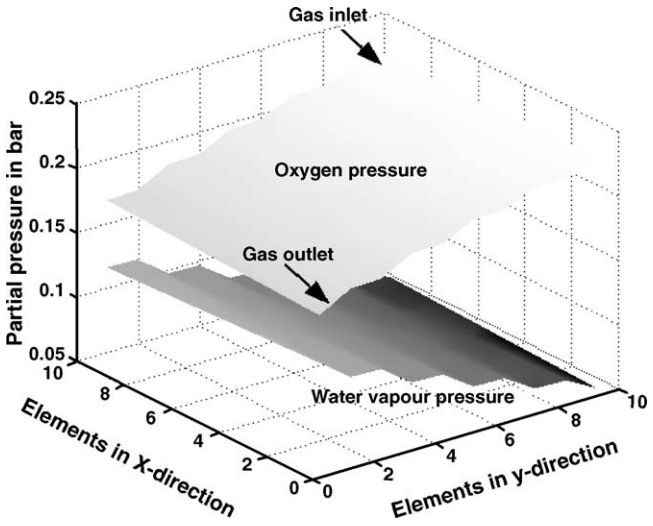

Fig. 3. Partial pressure of oxygen and water in the flowfield.

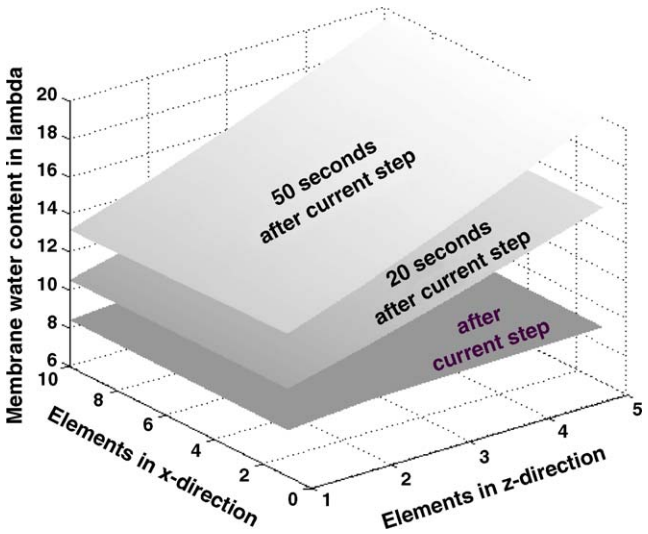

Fig. 5. Membrane water content.

2.6.1. *Influence on partial pressure*

The partial pressure of oxygen and the water vapour pressure in the flowfield are shown in Fig. 3 for a current density of 0.8 A cm^{-2}. The calculation was done with 10 elements in x and y direction. In this case the oxygen pressure is decreasing along the gas channel of the meander from the inlet to the outlet. The water vapour pressure is increasing from the inlet to the outlet.

The GDL is simulated within several layers. As shown in Fig. 4 the oxygen partial pressure in the layer next to the catalyst layer is always higher than 0.1 bar at a current density of 0.8 A cm^{-2}. The oxygen pressure is increasing according to the flowfield. During these conditions there was also liquid water in the GDL. However, the amount was low and did not lead to a significant reduction of reactive gases.

2.6.2. *Membrane performance*

The performance of the cell is strongly influenced by the resistance and the water content of the membrane. The equations of the membrane model are based on Nation® as well known material. The parameters of the used Gore membrane are different to Nation® and so during the calculations a parameter fit was necessary.

In Fig. 5 the amount of water is presented for three different times during the simulation in the x–z layer. The amount of water before the current step at 0.05 A cm^{-2} is almost equal in the membrane and low, because of minor water production. Twenty seconds after a current step the amount of water is increasing because of the high current density (0.80 A cm^{-2}). After 50 s, the transients are almost decayed and the water content of the membrane is higher near the cathode than at the anode.

The change of the membrane resistance in x–y direction for the same current step is shown in Fig. 6. The influence of the meander flow-field on the water amount leads to high differences in the membrane resistance. The average value of the resistance before the current step is about five-times higher than 50 s after the current step.

The current density is not constant because of an inhomogeneous resistance in x–y direction (Fig. 6). At an average density

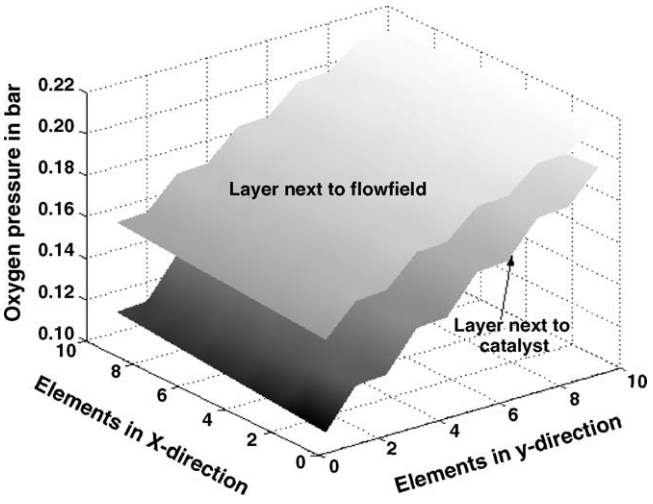

Fig. 4. Partial pressure of oxygen and water in GDL.

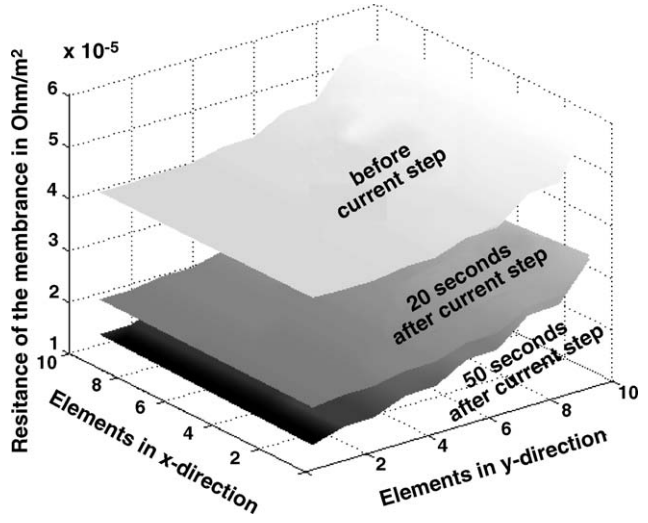

Fig. 6. Resistance of the membrane.

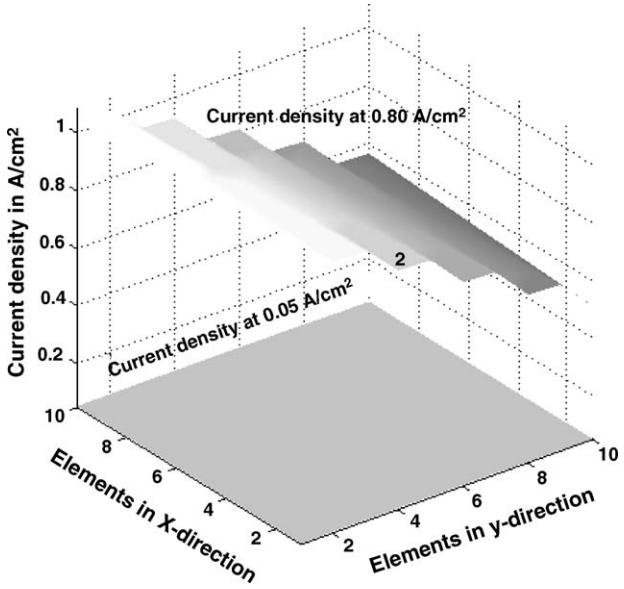

Fig. 7. Local current density.

of 0.05 A cm^{-2} the current density (Fig. 7) is not varying a lot. At higher currents the membrane acquires a high local current density. At 0.80 A cm^{-2} the highest local current density is up to 1.00 A cm^{-2} and the lowest is only about 0.50 A cm^{-2}. This leads to higher voltage losses at the membrane and a lower cell voltage. This influence is dynamically described in the next paragraph.

2.6.3. Dynamic behaviour

The comparison of the dynamic behaviour of the fuel cell model and the measurement are presented for a relative humidity at the cathode of 80% and at the anode of 20%. The stoichiometry was 4 at the cathode and 2 at the anode. The cell voltage of the simulation is compared in Fig. 8 with the measurement for dynamic loads. The presented voltages are standardised. The figure shows always an excellent agreement between measurement and simulation.

After a current step to higher values the voltage is at first decreasing sharply, then increasing in the next 60 s to its stable value. This behaviour can be explained by the humidity change of the membrane, which is increasing, because of the water production during high current. Switching back to lower current values the membrane is drying out and the voltage is decreasing after the first few seconds.

3. HIL test benches

For the development of fuel cell stacks or fuel cell systems, there is an increasing need in suitable test benches. The MAGNUM company has been one of the first suppliers of fuel cell test benches and in particular of HIL capable test benches. The advantage of using HIL test stands is that already in an early stage of development testing of whole system can be performed, even though not all the hardware is available. The following Fig. 9 shows the configuration of a conventional test stand.

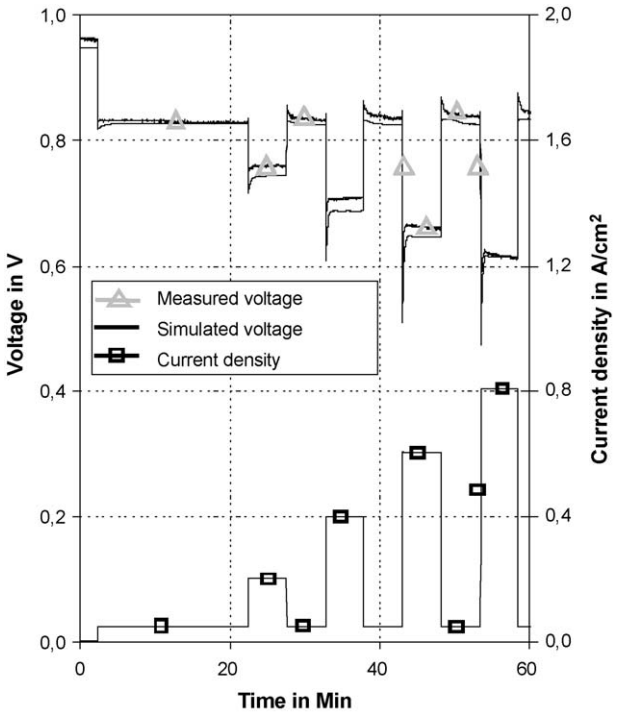

Fig. 8. Comparison measurement and simulation.

As shown in Fig. 9 the whole fuel cell system can only be tested if all sub-systems and units are available. In contrast, Fig. 10 shows the configuration if there is a possibility to integrate HIL simulation.

As demonstrated in Fig. 10 it is now possible to replace defective or unavailable components with their mathematical models and perform analysis of operational behaviour of the fuel cell system.

Because of the possibility to operate the hardware together with simulation models one of the main aspects for the realisation of HIL test stands are the safety requirements. A high safety standard is reached through the implementation of multistage switch off procedure on the PLC (Fig. 10). Furthermore, a plausibility check is done by the PLC for the set values of the controllers calculated in the model, before being passed on to the hardware. The PLC will restrict the set values to reasonable limits and prevent dangerous operation conditions. This is especially important in case of, e.g., mixing hydrogen and oxygen on the anode side, or when calculating the pressure set values by the model.

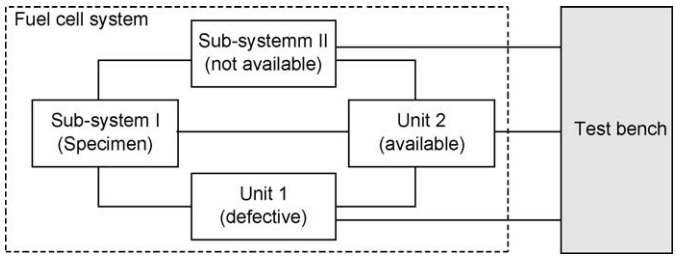

Fig. 9. Conventional test bench.

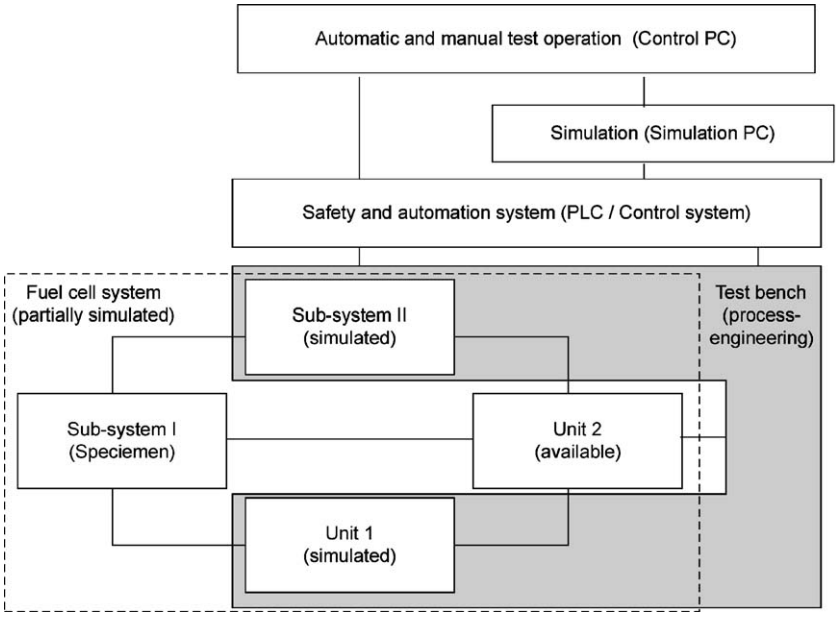

Fig. 10. HIL capable test bench.

Another important aspect regarding automotive applications is the dynamic operation of the test bench. Therefore, fast mass flow and pressure controllers are integrated and also fast data acquisition and data exchange between the PLC and control PC, respectively, simulation PC are realised.

In order to afford dynamic changes of the gas humidification in the test stand, model based control algorithms are implemented. Thermodynamic simulations have been integrated to develop new control algorithms for temperature and moisture. These methods allow to determine the actual moisture with high accuracy, by measuring solely temperature and considering heat capacities of gases and equipment.

Fig. 11 gives an overview of the general configuration of the above described test bench and the interaction of the test stand with the control and simulation PC.

As shown in Fig. 10 the fast data transfer between the automation PC, HIL computer and the PLC is realised via ethernet connection. The HIL simulation can be started by the operator choosing an adequate operation mode on the automation PC. The simulation model is running on the HIL PC in real time writing selected set values to the PLC and simultaneously reading actual values from PLC.

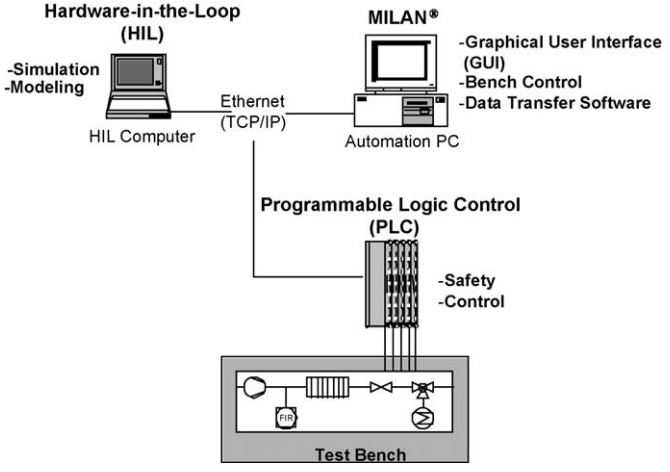

Fig. 11. Automation and data transfer within HIL test bench.

3.1. HIL fuel cell vehicle simulation system

In case of system simulations and HIL applications with regard to computational time a one-dimensional PEMFC model is used, which is implemented in MATLAB/Simulink. The main model outputs are cell voltage, temperature as well as electrical and thermal power, which are calculated with respect to different operating conditions, such as load current, pressure, flow, gas composition, moisture, etc. The vehicle model consists of the commercially available simulation tool CarSim where the internal combustion engine is replaced by a model of an asynchronous motor and an inverter.

After the model based analysis the HIL vehicle system is introduced, which allows investigating the behaviour of the real components in a virtual environment. The main components of the fuel cell HIL system, their properties will be described in detail, are the command station, target node PC with real time operating system, signal-conditioning unit, device under test and, for presentation purposes, a separate human machine interface consisting of a steering-wheel and a break and a throttle pedal.

3.1.1. Fuel cell vehicle model

CarSim, the fuel cell vehicle model, provides the complete vehicle dynamics. The power unit consist of an electric motor, an inverter model and a fuel cell model. Fig. 12 gives an overview of the model and the interactions between different model parts.

Via the throttle the required torque is predetermined. The power demand, which is needed for the required vehicle speed is

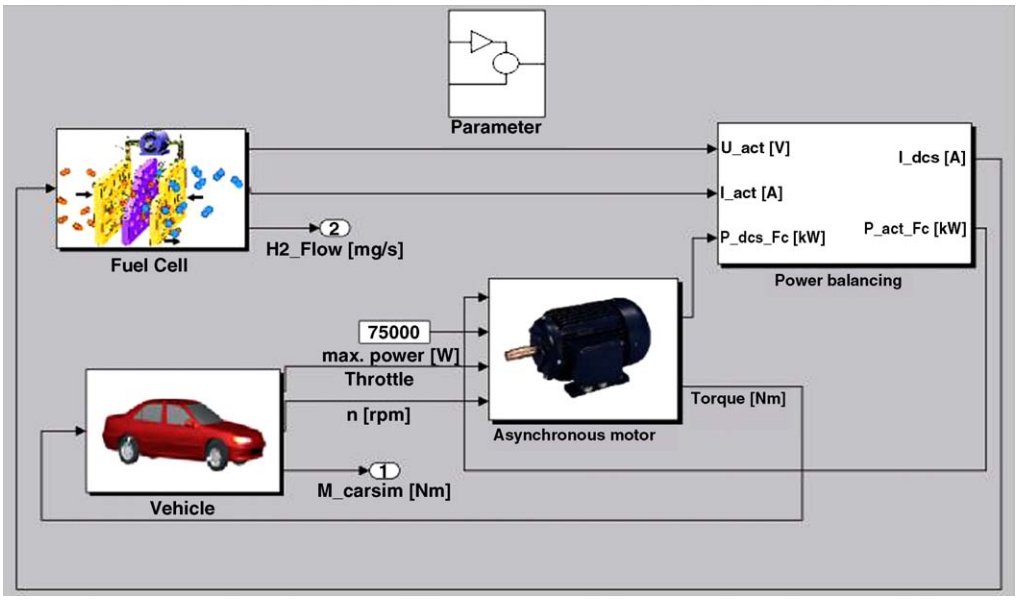

Fig. 12. Overview of the fuel cell vehicle model.

calculated from the vehicle model, the aerodynamic and friction forces. This power demand is provided to the fuel cell model where the actual power according to the prevailing operational conditions is calculated and provided via the inverter model to the model of the asynchronous machine. The propulsion torque is transmitted via one-step gear to the CarSim vehicle model. Below the different parts of the model are described in detail.

3.1.2. CarSim vehicle dynamics model

CarSim is a commercial program for vehicle dynamics. It provides different precompiled vehicle models, for example dynamic link libraries, which can be easily included in the Simulink models. It also includes a scientific plotter and an animator for displaying the results. The animator is able to work in real-time, so it is possible to build up driving simulators. 2D and 3D tables, unlimited in length, parameterise the vehicle models.

The CarSim model includes:

- A wide range of controllers for braking, steering (for example a driver model), gear shifting and for event handling.
- Wind and aerodynamic effects (six aerodynamic forces and moments can be applied to the sprung mass).
- 3D road geometry and friction.
- A full nonlinear kinematical behaviour of the suspension.
- Different tire models like Pacejka 5.2, Shear.
- A power train model for front-, rear- and four-wheel drive.

The model consists of 10 bodies and 27 degrees of freedom. Fig. 13 gives an overview about different modelled motions of the vehicle.

The different bodies are one sprung body, two unsprung bodies, rigid axle stroke, rigid axle rotation, four spinning wheels and engine crankshaft.

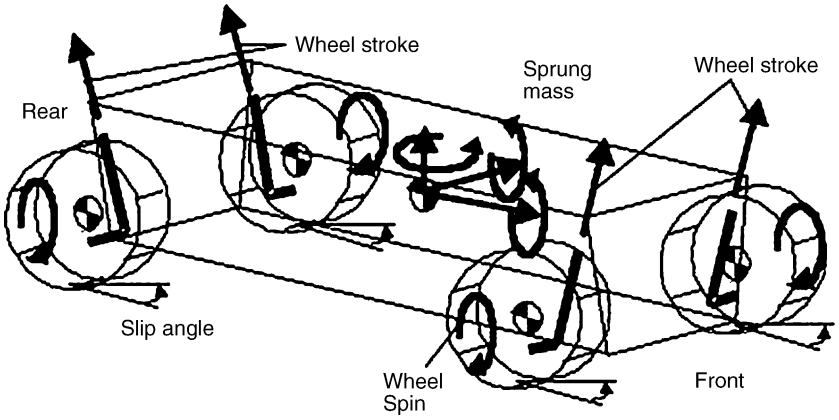

Fig. 13. Degrees of freedom of the CarSim vehicle model.

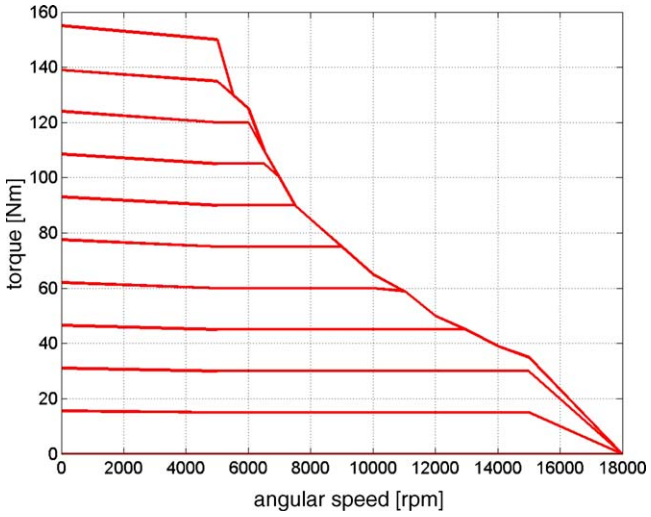

Fig. 14. Characteristic map of asynchronous motor.

If the vehicle model is used in Simulink one can export approximately 530 variables and import about 150 to expand the vehicle models with controllers or vehicle parts. Especially for the HIL application CarSim RT includes models to be implemented into specific real-time platforms, like dSpace, RT-Lab, ADI and more. A more in depth description would be beyond the scope of this article due to the complexity of the model. An extensive description can be found in literature [5,6].

3.1.3. Motor and inverter model

By default CarSim offers the possibility to choose between different internal combustion engines (ICE), which are represented by their characteristic map. In order to use CarSim together with a fuel cell as a power source, the ICE is replaced by the model of an electrical motor and inverter.

The model of an asynchronous motor combined with a standardised inverter is employed because of the high development stage. Characteristic maps as shown in Fig. 14 describe the behaviour of the motor and inverter.

Fig. 15 illustrates how the power unit reacts on applying the throttle pedal by the driver. The part marked blue represents thereby the motor model.

The driver applies the throttle, whereas a final controlling element translates the input to a claimed torque. Although the driver applies the throttle to reach a specific speed, the throttle control requests a torque. The driver acts as a superposed speed controller. The torque of the engine is obtained from the angular speed of the engine and the characteristic curve of the torque, Fig. 14.

The requested torque together with the actual angular speed of the electric drive provides the requested power. In the block "Power balancing" the power is limited by the maximum available power of the motor. Before entering the fuel cell model the requested power is corrected for losses of inverter and motor by the efficiency map. Finally, the fuel cell stack is loaded with this requested power and drives the motor. The model can eas-

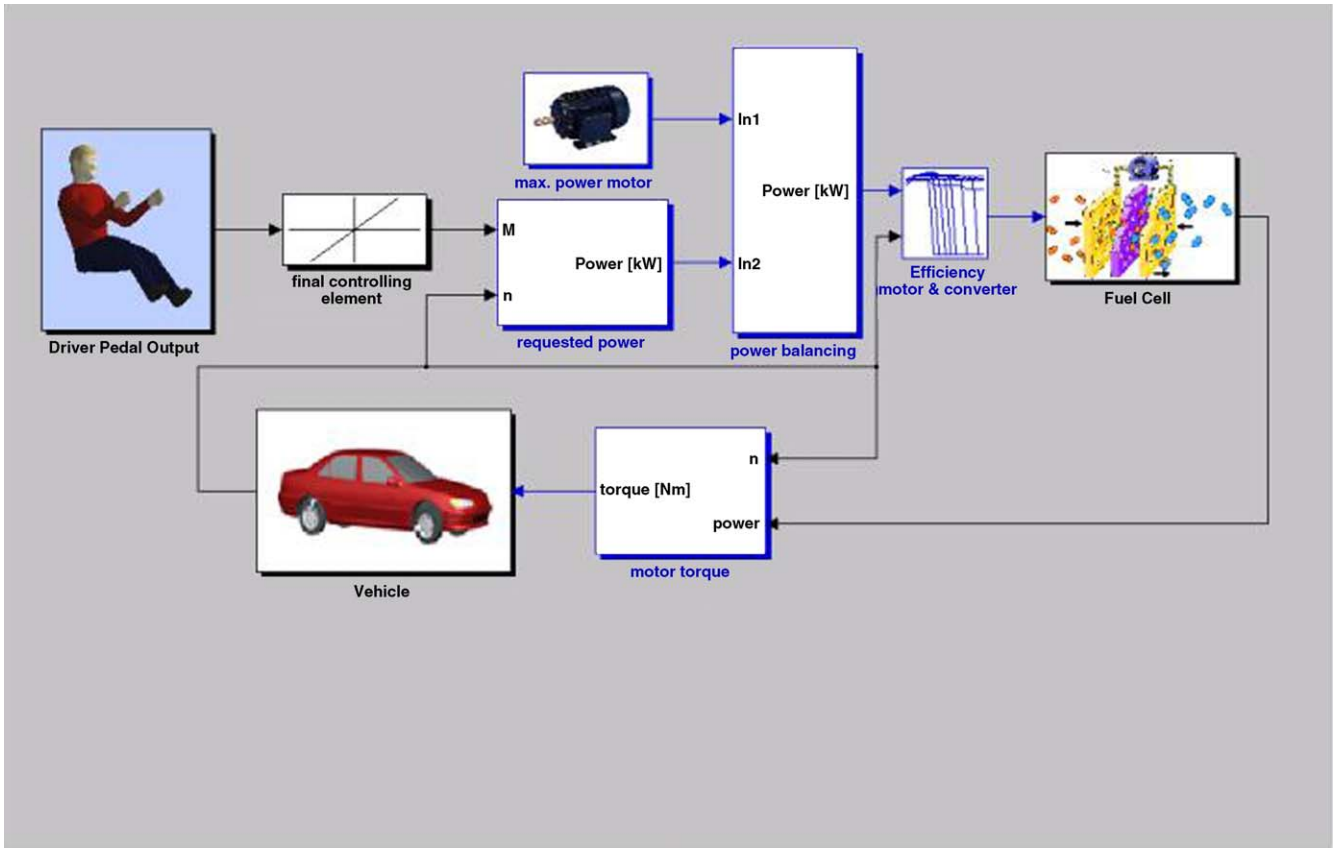

Fig. 15. Overview of the motor and inverter model.

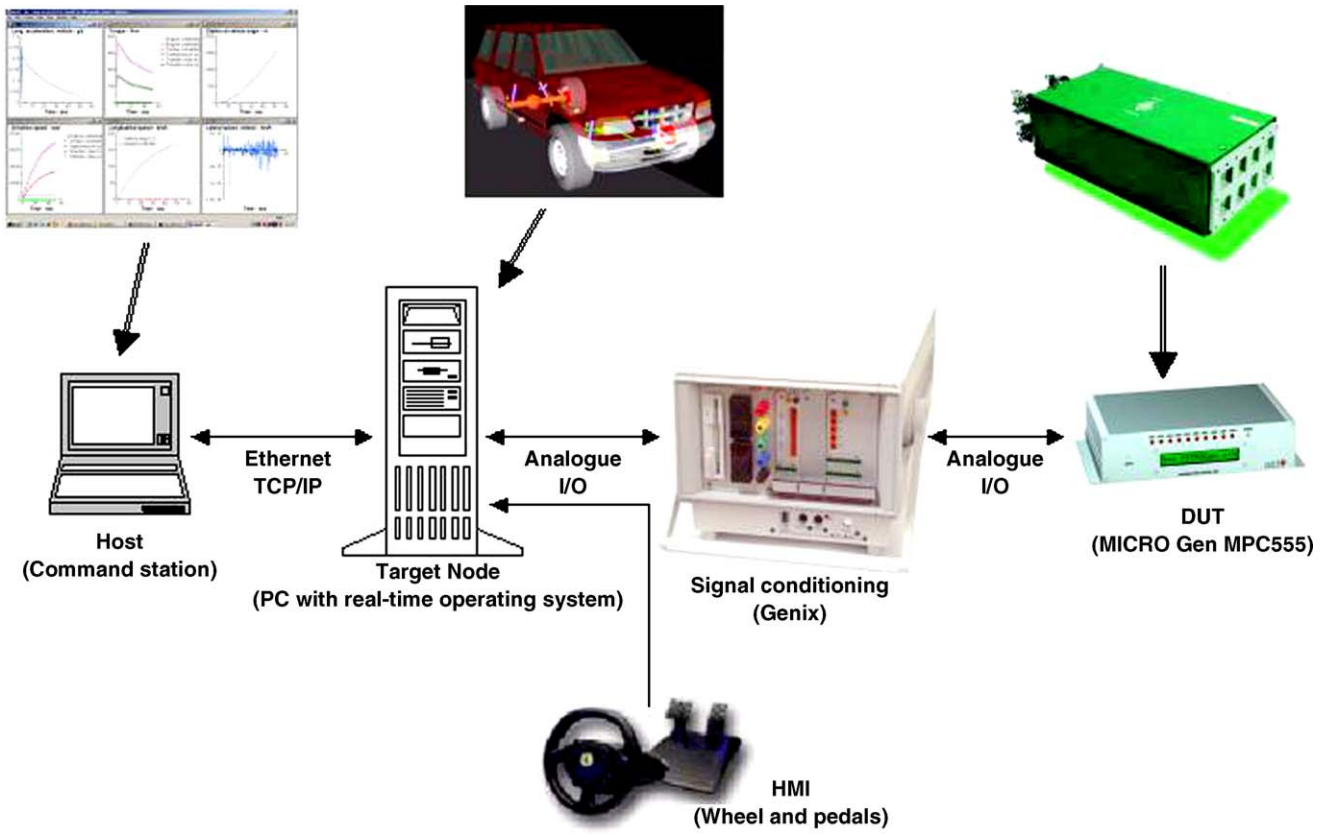

Fig. 16. Overview of the motor and inverter model.

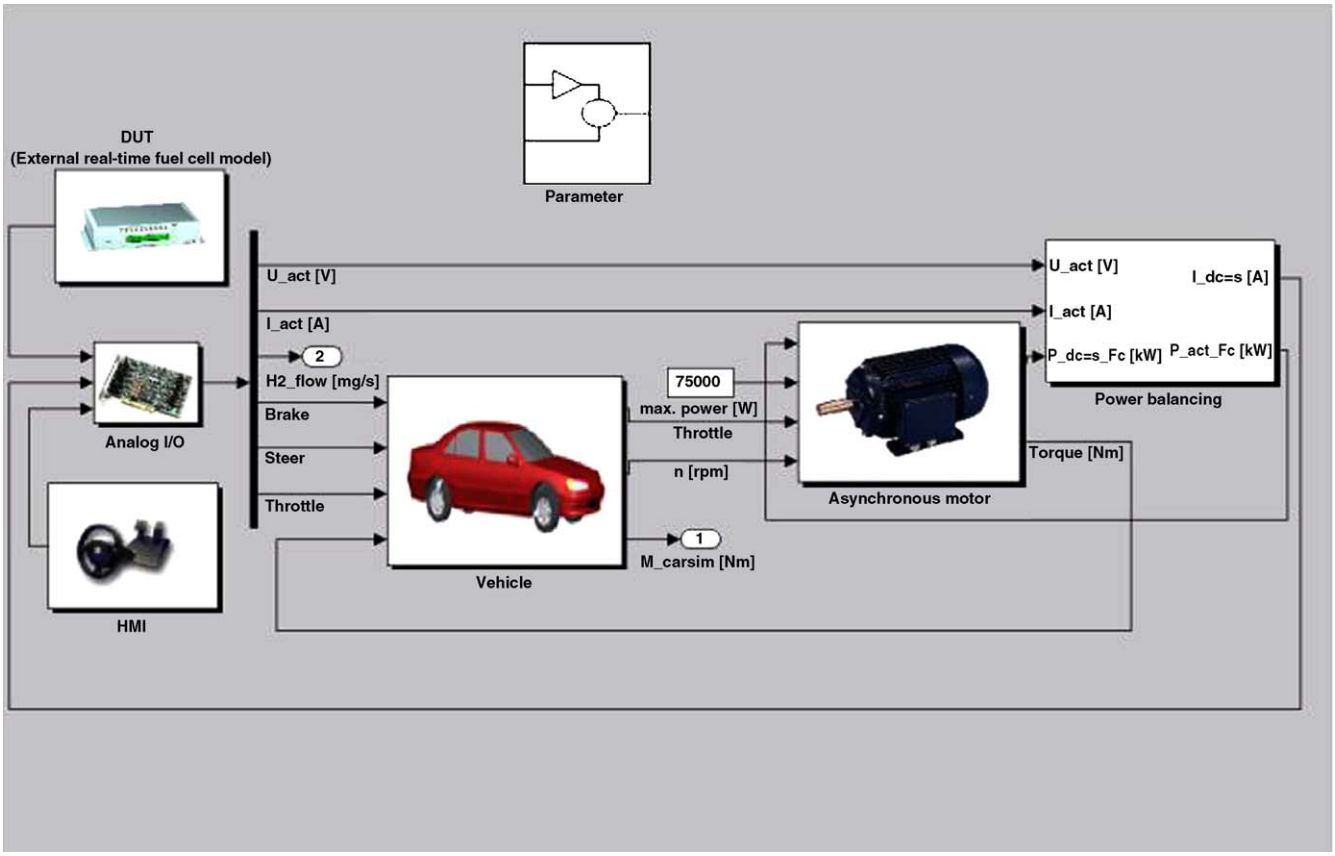

Fig. 17. HIL application for a fuel cell vehicle.

ily be extended if there is a need for more detailed electrical, mechanical or thermal models of the motor and inverter.

3.1.4. One-dimensional fuel cell stack model

The one-dimensional fuel cell model used in this work is described in more detail in references [7–9]. Different layers of the fuel cell (Fig. 1) with their different physical and electrochemical characteristics are implemented in the one-dimensional model.

The main equations describing the dynamic behaviour are given in Chapter 2. In contrast to a described three-dimensional model here the discretization is done only perpendicular to the species flow, whereas all the channels in the flowfield are summed up to one volume.

4. HIL set-up

The following chapter gives an overview of the HIL system and the resulting advantages for the development process.

The HIL system consists of the command station, target node PC with real-time operating system, signal-conditioning unit, device under test and a separate human machine interface (HMI) consisting of a steering-wheel and a break and a throttle pedal (Fig. 16). The HMI allows user to interact directly with HIL system and to "drive" the fuel cell car in a 3D environment.

The command station communicates via ethernet with the target PC where the vehicle model including inverter and electric motor model is running in real-time. Via analogue I/Os the target PC communicates with the device under test (DUT). In this case the DUT plays the role of a fuel cell stack and gas supply units, which are also "simulated" and running in real-time on a micro controller MICROGen MPC555. This arrangement is chosen in order to minimise the development costs of the HIL system. In a real application the HIL capable test bench where the above-mentioned components are real existent could easily replace the micro controller.

MAGNUM is a leading company in the area of HIL capable test benches for fuel cells and components, further details about MAGNUM's fuel cell HIL test benches can be found in [9,10].

Between DUT and target PC a signal-conditioning unit (Genix) is introduced in order to adjust the signal amplitudes in needed range.

The HMI enables the user to drive a vehicle like a real car with familiar operating elements.

Fig. 17 shows the application of the HIL concept for the fuel cell vehicle, In contrast to the fuel cell vehicle model (Fig. 12), it can be recognised that the fuel cell stack is not a part of the model any more. The fuel cell stack acts now as DUT and exchanges data with vehicle model via analogue I/Os. The interface between HMI and the vehicle model is also presented in Fig. 17.

System analysis and optimisation combining the real existing hardware (DUT) with simulation models can be done using the HIL set-up shown in Fig. 17. It is obvious that, e.g., the power unit, which is an integral part of DUT, can be tested in the simulated vehicle environment. The advantage is that before the design of packaging the power unit with its components can be tested and optimised in a user-friendly environment, e.g., easy accessibility of components in a test bench, etc. Different hardware configurations can be tested and their influence on the dynamic behaviour of the vehicle and also the fuel consumption can be analysed.

Fig. 18. HIL application for a fuel cell vehicle.

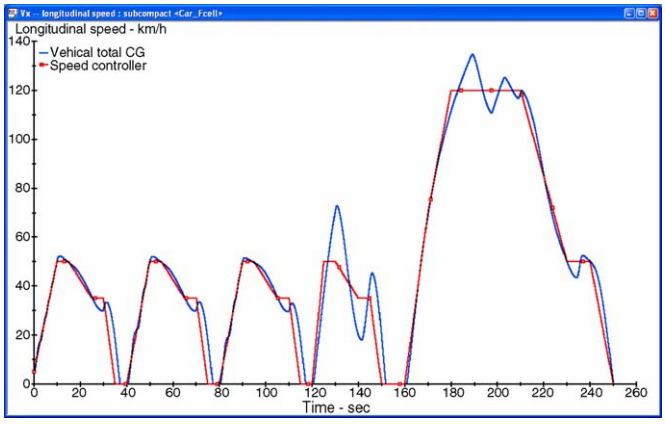

Fig. 19. Vehicle speed.

Another important application of the HIL simulation is the model validation in real time. With obtained measured data from the real stack, parameter optimisation of the stack model can be performed. Validated real time fuel cell system models can be used for model-based controller development [11].

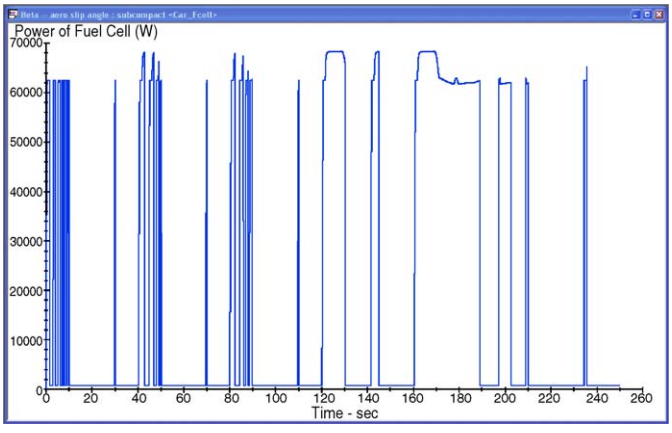

Fig. 20. Fuel cell power.

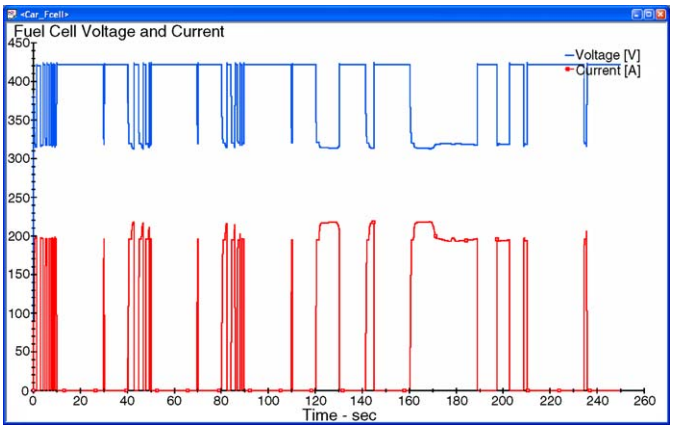

Fig. 21. Stack voltage and current.

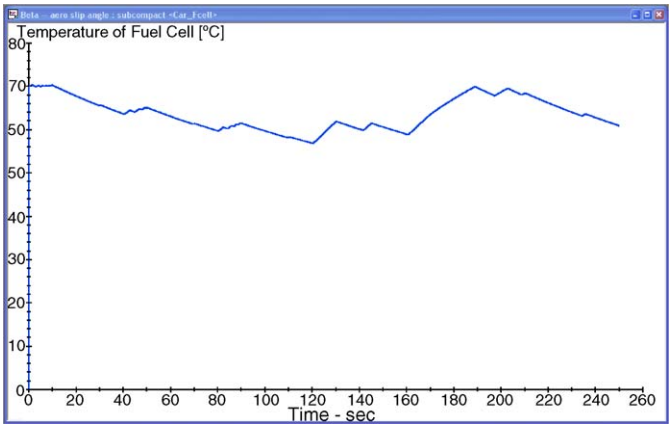

Fig. 22. Stack temperature.

Increased flexibility of the development process is another great advantage. Consecutively, the different component models can be replaced by their hardware leading to an optimised system.

5. HIL simulation results

Several examples of results obtained from the HIL simulation are presented below. Fig. 18 shows the vehicle and road set-up used for the simulation.

In the following figures (Figs. 19–22) results from a certain driving cycle are shown. Fig. 19 shows the profiles of the input for the speed controller and calculated speed by the vehicle model (Vehicle total CG). In Fig. 20 the actual value of stack power is presented. The response of the stack voltage, current and temperature are shown in Figs. 21 and 22.

6. Summary

The dynamical 3D model has been developed to describe the partial pressure in the flowfield and GDL dynamically. The change of membrane resistance with dynamic load and the resulting local current density is evaluated within the model. The results for the dynamic behaviour of the PEMFC show excellent conformance with the measurement. They provide the bases for the HIL system model.

The presented HIL system used as development platform offers significant advantages compared to conventional test systems. Using the presented model, consisting of vehicle dynamics, electric motor and inverter and a fuel cell stack a wide range of system designs can be tested.

The introduced HIL set-up allows to replace certain component models by their hardware and the whole system behaviour can be analysed under real-time conditions. Furthermore the HIL system offers the possibility to run models in parallel to the investigated hardware and to validate and optimise the models, as well as to use the models as diagnostic tools.

References

[1] D. Bernardi, M.W. Verbrugge, Mathematical model of a gas diffusion electrode bonded to a polymer electrolyte, AIChE J. 137 (8) (1991 August) 1151–1163.
[2] M. Wöhr, Instationares Thermodynamisches Verhalten der Polymermembran Brennstoff-zelle, Dissertation, Fortschritts-bericht VDI Reihe 3 Nr, 630 Düsseldorf VDI, Verlag, 2000.
[3] H. Wendt, G. Kreysa, Electrochemical Engineering, Springer-Verlag, Berlin Heidelberg, 1999.
[4] T.E. Springer, T.A. Zawodzinski, S. Gottesfeld, Polym. Electr. Fuel Cell Model J. Electrochem. Soc. 138 (8) (1991 August).
[5] CarSim Reference Manual, Version 6, Mechanical Simulation Corporation, 2004.
[6] T.D. Gillespie, Fundamentals of Vehicle Dynamics, Society of Automotive Engineers, Warrendale, PA, 1992.
[7] Z. Lemeš, Modellbildung und Simulation des Dynamischen Verhaltens einer Polymer-Elektrolyt-Membran-Brennstoffzelle, Shaker Verlag, Aachen, 2005.
[8] Z. Lemeš, A. Vath, Th. Hartkopf, H. Mäncher, Dynamic Fuel Cell Models and their Application in Hardware-in-the-Loop Simulation, 9th Ulm Electrochemical Talks, 2004. (Also to be published in a special issue of J. Power Sources, 2005.).
[9] Z. Lemeš, Modellbasierte Untersuchung des Betriebsverhaltens einer Polymer -Elektrolyt-Membran-Brennstoffzelle, VDI-Berichte Nr. 1828, 2004.
[10] H. Mäncher, H. Manske, Hardware-in-the-Loop-taugliche Brennstoffzellen-Prüfständeals Entwicklungsplattform, VDI-Berichte Nr. 1828, 2004.
[11] E. Ramschak, J.H. Thanner, M. Schuessler, P. Prenninger, Application of HIL Test Bench for SOFC System Development, Lucerne Fuel Cell Forum, 2004.